Experimental investigation of the aerodynamic characteristics of generic fan-in-wing configurations

N. Thouault, C. Breitsamter and N. A. Adams
Institute of Aerodynamics
Technische Universität München
Garching, Germany

C. Gologan and J. Seifert
Bauhaus Luftfahrt e.V.
Garching, Germany

ABSTRACT

This experimental investigation concentrates on the aerodynamic behaviour of a generic fan-in-wing configuration. The effects of the fan(s) on the flow circulation in a short take-off and landing or a transition flight condition without ground effect are evaluated. A wind-tunnel model has been constructed and tested to quantify the aerodynamic effects. Force measurements, surface pressure measurements, stereo-particle image velocimetry and wool tufts flow visualisation are performed. Different fan-in-wing configurations with the fans rotating in the wing plane, one fan either at the rear or front part of the wing and two fans are compared to the closed wing without fans set as reference. A fan placed near the trailing edge improves significantly the lift coefficient due to a jet flap effect on the wing lower side combined with enhanced suction on the wing upper side. The jet exiting the nozzle rolls up in a counter rotating pair of vortices affecting significantly the wing behaviour.

This experimental investigation constitutes also a useful database for further CFD comparison.

NOMENCLATURE

C_D	drag coefficient
C_L	lift coefficient
C_{Lref}	reference lift coefficient of the closed wing configuration
C_m	pitching moment coefficient with respect to the quarter chord
C_p	pressure coefficient
c	root chord
L	lift
D	drag
D_E	equivalent drag
N	fan rotational velocity (RPM)
R	fan radius
Re_c	Reynolds number based on the root chord
s	wing span
T	fan static thrust
t	maximum wing thickness
u	streamwise velocity component
V_∞	freestream velocity
x,y,z	streamwise, spanwise and transverse coordinate directions
ΔC_L	incremental lift coefficient ($C_L - C_{Lref}$)
μ	tip-speed ratio
θ	circumferential pressure taps angular position
PIV	particle image velocimetry
STOL	short take off and landing
VTOL	vertical take off and landing
CFD	computational fluid dynamics
URANS	unsteady Reynolds averaged Navier-Stokes

Paper No. 3338. Manuscript received 15 August 2008, accepted 10 November 2008.

https://doi.org/10.1017/S0001924000002736 Published online by Cambridge University Press

1.0 INTRODUCTION

The fan-in-wing concept was originally designed to fulfill VTOL requirements. It was successfully implemented in the experimental aircraft GE-Ryan XV-5 in which a lift-fan was installed in the plane of each wing and one in the fuselage nose for pitch control. A fuselage lift-fan is also currently used in the F-35 B for longitudinal stability purposes. Aerodynamic effects due to the interaction of the fan with the freestream could provide advantages for STOL to reduce the transition flight stability issues encountered from hover to cruise conditions, especially for a possible implementation in a regional civil aircraft. Induced lift is of interest to reduce the lift fans' thrust requirements and therefore reduce the corresponding mass with respect to cruise conditions. Following a fan-in-wing concept recently proposed[1], the fans are installed near the root section mainly for structural reasons. The wing root gives also the maximum thickness to install fans of relevant size. The fans are used only for take-off and the fan inlet and exit are sealed during cruise.

A number of experimental investigations can be found in NASA technical notes. Many of them are related to the development of the Ryan GE XV-5 experimental aircraft. In 1959, Hickey *et al*[2] presented experimental results of a semi-span wing model with a large fan rotating in the plane of the wing. In this study, the experimental setup and mainly the fan engine shaft constituted an important flow disturbance source. In 1963, Hickey and Hall[3] tested a large-scale model with one fan placed in each wing. In 1964, Hall *et al*[4] investigated the aerodynamic characteristics of a full scale fan-in-wing model including a nose fan for pitch control. Similarly, Kirby and Chambers[5] investigated the dynamic stability and control characteristic of a 0·18-scale VTOL fan-in-wing aircraft in 1966. Several studies have been carried out in ground effect for a VTOL fan-in-wing aircraft. In 1968, Oberto *et al*[6] analysed the performance of a multi-fan-in-wing transport model. Three fans of different diameters were located one next to the other in the wing spanwise direction. In 1974, Heyson[7] investigated the effect of wind-tunnel wall on the performance of a VTOL fan-in-wing aircraft. Another study of a VTOL fan-in-wing wind-tunnel model in ground effect was also conducted by Wilson *et al*[8] in 1996. An overview of the influence of the ground on various VTOL concepts was proposed by Schade[9]. An investigation has been conducted on flow distortion in fan-in-wing inlets by Schaub[10] in 1968. Flow distortion at the fan inlet is a critical issue for a fan-in-wing configuration. Inlet guide vanes above the fan inlet can reduce the inflow distortion and improve the fan performance[11]. The back pressure at the fan exit was also found to significantly affect the fan performance [12]. Results obtained with different fan-in-wing wind-tunnel models were compared by Hickey[13-14]. The effect of the fan streamwise position was discussed while comparing these models with different planforms. Surveys[15-18] on the lift-fan technology provide a good summary of the work done at NASA on this topic.

Here, a generic wind-tunnel model has been built to investigate several generic configurations: (*i*) the closed wing without fan set as reference, (*ii*) one single fan installed either at the rear or at the front part of the wing and (*iii*) two fans placed symmetrically with respect to the half chord. A schematic drawing of the wing in which a single fan is placed at the rear part is presented in Fig. 1. A part of the incoming flow is ingested by the fan and expelled at the fan exit, consequently creating a cross-flow problem.

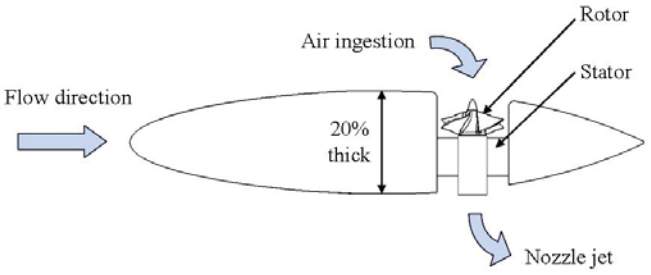

Figure 1. Principle sketch of the fan-in-wing concept.

The present study provides first data to investigate the implementation of this concept to a STOL regional aircraft and focuses on describing the major phenomena. Therefore, no guiding vanes or deployable seal are included in the wind-tunnel model. For a single fan-in-wing configuration, the aerodynamic influence of the fan position on the wing is studied. Considering a two fan-in-wing configuration, with one fan next to the other in the streamwise direction, the jets' interference is discussed. The results are systematically compared to the wing without fan to assess the aerodynamic influence of the cross-flow generated by the fan on the lifting surface. Finally, qualitative and quantitative data are gathered to set up a data base for further CFD comparison.

2.0 EXPERIMENTAL SETUP

A specific wind-tunnel model was designed and constructed for this investigation. A NACA 16-020 aerofoil is used giving a relative thickness of 20%. This thickness ratio was chosen to provide enough space to insert the two fans inside the wing. The semi-span wing model has an aspect ratio of 2·3, a semi-span area of 0·683m², a taper ratio of 0·71 and 0° sweep of the 0·5 chord line.

No specific optimisations were made on the model which was designed to give the possibility of investigating several generic fan-in-wing configurations: (*i*) the closed wing without fan set as reference, (*ii*) one single fan installed either at the rear (Fig. 2) or at the front part of the wing and (*iii*) two fans placed symmetrically with respect to the half chord as shown in Fig. 3.

The model is installed with a peniche to place the semi-span wing out of the wind-tunnel wall boundary layer. The peniche shape has a constant profile identical to the wing root chord. The peniche height has been chosen to obtain approximately two fan diameters between the wind-tunnel floor and the lower point of the inlet lip. With the model mounted on such a peniche, the influence of the floor is supposed to have a non significant effect on the cross-flow.

The fans' axis positions are located at ⅓ chord for the front fan and ⅔ chord for the rear fan; both located at a relative spanwise position of 0·12s measured from the wing root chord. Both fans are identical with a diameter of 120mm. On the wing upper side, the ratio of inlet lip radius to diameter (Fig. 4(b)) was set to 8% to keep a reasonable wing thickness. The fans are composed of two stages, a four-blade rotor and four-blade stator. The engine is located inside the stator hub and therefore gives a relatively realistic model with no exterior devices that could disturb the flow. Only the cables to provide power and to measure the engine temperature are a source of disturbances. These cables are located behind one stator blade trailing edge (Fig. 4(a)) to minimise their influence.

The fans used during this experiment were originally employed for radio/controlled modelling purposes. The maximum rotational speed that one could achieve is about 26,500rpm corresponding to a static thrust of T = 40N (measurement made at zero airspeed). The disadvantage of these fans is that the rotational speed cannot be kept fully constant and consequently varies to some extent during the measurements. This variation depends mainly on the power provided to the fan, changing with fan interference and angle-of-attack. The uncertainty interval of the fan rotational speed for the three different rotational speeds investigated is as follows: N = 21,000rpm ± 200rpm, N = 23,700rpm ± 500rpm and N = 26,500rpm ± 500rpm. In the next sections only the average rotational speed is noted. The fan rotational speed was measured for most of the operating point using a laser tachymeter.

https://doi.org/10.1017/S0001924000002736 Published online by Cambridge University Press

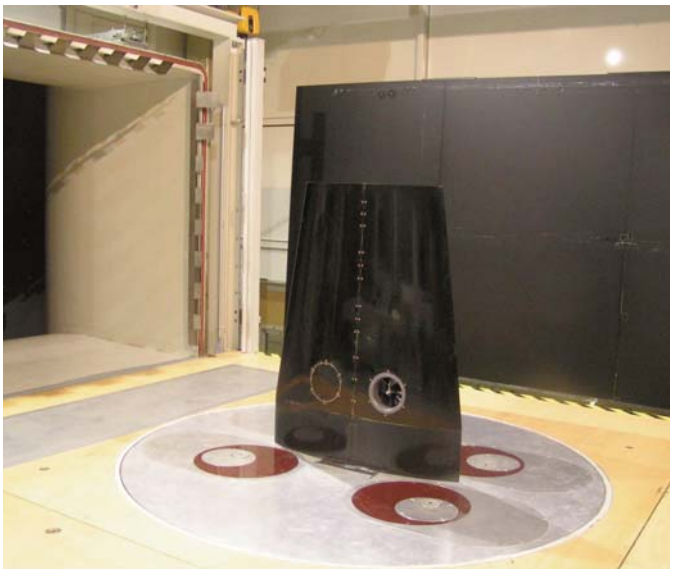

Figure 2. Fan-at-rear configuration in wind tunnel.

Figure 3. Two-fan in wing configuration.

The wind-tunnel inlet section is 1·80m*2·40 m and the floor length is 4·80m. The measurements are preformed in an open test section. The maximum achievable speed is 65ms^{-1} and the working section turbulence level remains under 0·4%. The tolerance on the angle-of-attack and side slip angle stays under 0·2°. Force and pressure measurements, PIV as well as flow field visualisation are carried out. The force measurements are conducted with an external 6 component underfloor balance. The balance precision is ±0·0022 for the lift coefficient, +0·0011 for the drag coefficient and ±0·0005 for the pitching moment coefficient.

For the fan-in-wing configurations, angle-of-attack polars are measured between $\alpha = -10°$ to $\alpha = 20°$. No measurements are performed at high angle-of-attack in the stall region. Indeed, at 26° angle-of-attack, all fan-in-wing configurations, as well as the closed wing, reach stall which consequently causes a pumping behaviour of the fan. Therefore no measurements were conducted in this area to prevent possible damages.

Figure 5 shows the pressure taps layout on a top view of the two fans in wing configuration. Three chordwise pressure distributions located at 0·12s, ⅓s and ⅔s from the root chord are investigated. Two circumferential pressure distributions, located at a 1·6*R* and 1·9R respectively from the fan axis, were studied on both upper and lower side of the wing. The circumferential coordinate system is given in Fig. 5. It is set positive as counterclockwise which is also the fan rotational sense. The pressure taps are connected via tubes to a Scanivalve multi channel system which is connected to a PC using DIAdem for data acquisition. The precision of the measurement device is ± 0·006 for the pressure coefficient.

In addition, flow field measurements are conducted using Stereo-PIV. These measurements are performed only for the fan-at-rear configuration, near the trailing edge and downstream of the fan exit to capture the disturbed flow field due to the jet in cross-flow.

Wool tufts flow visualisation technique is employed for all configurations for a wide range of operating points. Wool tufts are positioned in the fan vicinity on both upper and lower side of the wing to analyse regions of attached and separated flow. Power measurements are also realised for a wide range of operating points: approximately 1kW required for the minimum and 2kW at the maximum rotational speed (respectively 21,000 and 26,500rpm). The fan engine could not be operated over 75°C. Thus, temperature measurements were made to check this parameter.

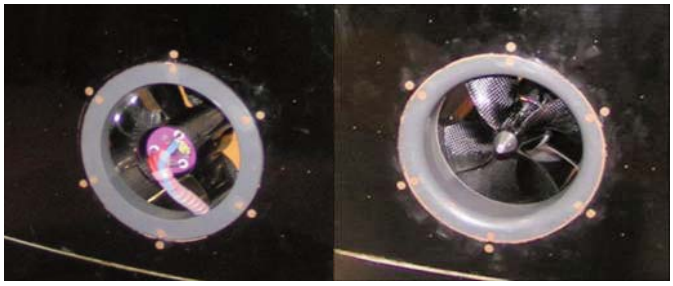

(a) (b)

Figure 4 (a) Fan exit, (b) Inlet lip.

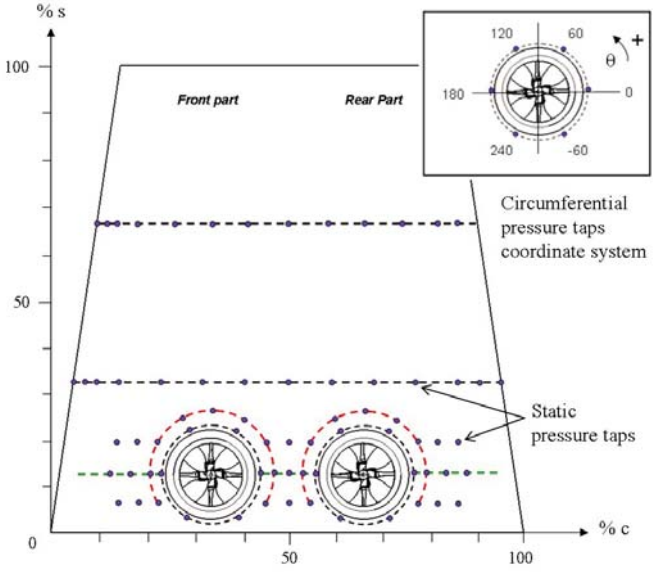

Figure 5. Pressure taps layout.

https://doi.org/10.1017/S0001924000002736 Published online by Cambridge University Press

3.0 RESULTS AND DISCUSSION

3.1 Force measurements

3.1.1 Configuration comparison

All the force measurements presented in this section have been conducted with a freestream velocity of 30ms^{-1} (Re_c = 1·5*10^6) and an average fan rotational speed of 21,000rpm which corresponds to a tip-speed ratio of μ = 0·227 as defined below in Equation (1).

$$\mu = \frac{V_\infty}{2\pi RN/60} \quad \ldots (1)$$

At this operating point, the fan rotational speed variation remains under 2% and has a small impact on the results. All fan-in-wing configurations have a strong effect on the aerodynamic coefficients. According to Fig. 6, the lift coefficient is increased compared to the reference case without fan. This becomes particularly true for the fan-at-rear configuration. In this case, the lift coefficient reaches twice the value of the fan-off configuration for α = 10°. In a single fan-in-wing configuration, the fan location (rear or front) has a significant influence on C_L. While increasing the angle-of-attack, the incremental lift coefficient, ΔC_L, is also increasing for the fan-at-rear configuration whereas the fan-at-front shows the opposite trend (Fig. 7). We can infer that when placing the fan closer to the trailing edge, a higher lift coefficient is achieved. Therefore, a fan installed in the wing generates an induced lift which is adding to the lift due to the angle-of-attack increase and to the fan thrust. Induced lift is defined as total lift minus aerodynamic lift due to angle-of-attack and fan thrust[15].

Continuing to Fig. 8, the drag coefficient rises significantly for all the fan-in-wing configurations. Above α = –3°, the fan-at-rear configuration gives a higher C_D than the fan-at-front configuration. Thus, the drag coefficient is also influenced by a fan location variation. The incremental drag coefficient tends to decrease at high angle-of-attack for the fan-at-front whereas it rises for the fan-at-rear configuration. Hence, the pressure drag depends on the fan location and also on the angle-of-attack for a single fan-in-wing configuration. When two fans are set inside the wing, the drag and lift coefficients appear to be an offset of the closed wing configuration. A definition of induced drag can also be introduced accordingly to the induced lift definition. Therefore the fan position clearly affects the induced drag. As stated before, the fan installed in the wing produces elevated lift compared to the reference case without fans. According to Fig. 9, this lift production comes with a significant drag. The lift over drag ratio remains considerably below the reference for the whole angle-of-attack range. At high angle-of-attack (α = 20°), the lift over drag ratios of the fan-in-wing configurations are comparable to the reference.

Fig. 10 presents the equivalent lift-drag ratio to account for the power needed to drive the fans. D_E is the equivalent drag obtained by dividing the measured power to drive the fans by the freestream velocity. This ratio gives more insight on the fan-in-wing configurations efficiency. The equivalent lift-drag ratio remains below 3 for the whole angle-of-attack range and for all configurations. The large amount of drag and equivalent drag contributes significantly to the penalty of driving the fans. Though, the efficiency is not as important as generating lift for a STOL aircraft for which the fans are only needed during take off.

The angle-of-attack polar of the pitching moment coefficient is presented in Fig. 11. The pitching moment reference point is the root chord quarter. The wing without fan is statically unstable for almost the whole angle-of-attack range. For the fan-at-rear configuration, the wing is statically stable above 8° and unstable below. Compared to the reference configuration, the fan-at-front induces a nose up moment, the fan at rear a significant nose down moment. The streamwise fan position affects notably the pitching moment because the fan induced lift has a strong impact also on pitching moment characteristics. For the two-fan configuration, C_m approaches the behaviour of the fan-at-front configuration for negative angle-of-attack. Above 8° angle-of-attack, C_m decreases and tends to approach the reference values.

To summarise, the fan position strongly affects the aerodynamic coefficients for a single fan-in-wing configuration: when shifting the fan toward the trailing edge, a higher lift and drag as well as a nose down pitching moment are observed. In contrast, the lift and drag are reduced and a nose up pitching moment is encountered when placing the fan closer to the leading edge. Therefore, the fan-in-wing configuration strongly influences stability issues. This is also the case for the rolling and yawing moments not presented in this paper. The circulation is enhanced by the presence of one fan installed at the wing rear part. The jet leaving the fan nozzle can be regarded as a thick jet flap. The previous conclusions about the fan location are consistent with the flap loading theory.

3.1.2 Tip-speed ratio variation

The aerodynamic coefficients depend on both the fan thrust and the freestream velocity. During the measurements, it was only possible to access the information concerning the overall model forces and

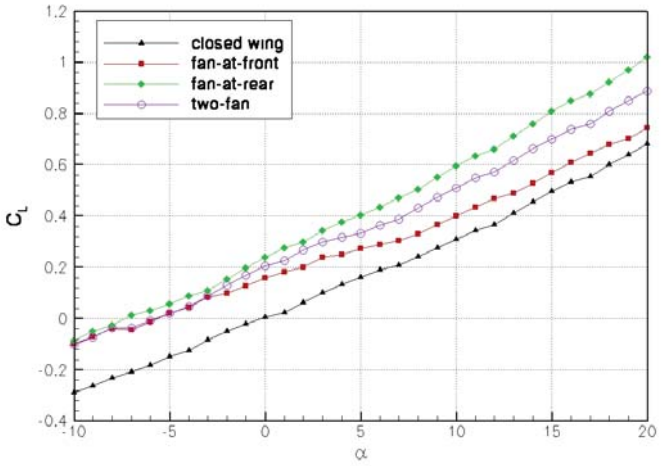

Figure 6. Lift coefficient comparison (μ = 0·227).

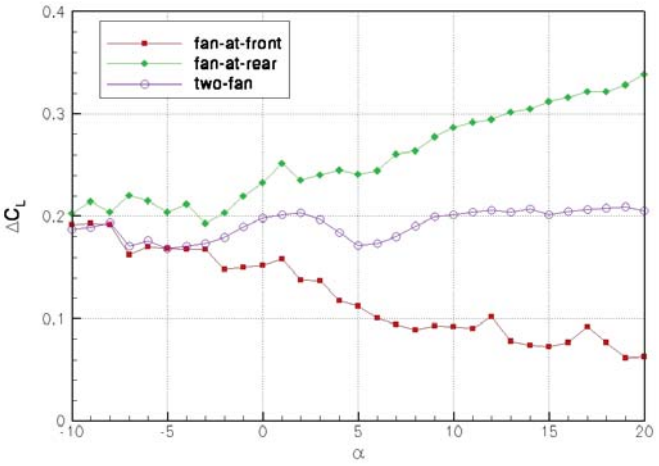

Figure 7. incremental lift coefficient comparison (μ = 0·227).

https://doi.org/10.1017/S0001924000002736 Published online by Cambridge University Press

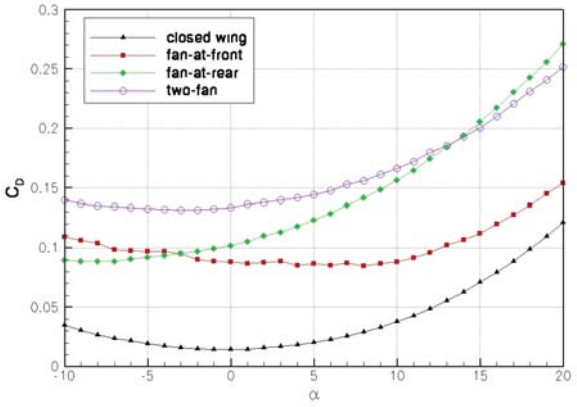

Figure 8. Drag coefficient comparison. (μ = 0·227).

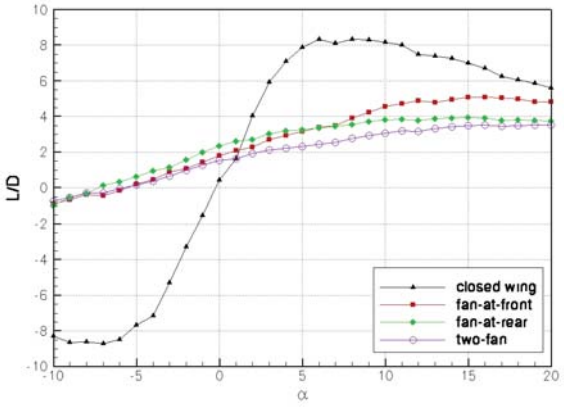

Figure 9. Lift over drag ratio. (μ = 0·227).

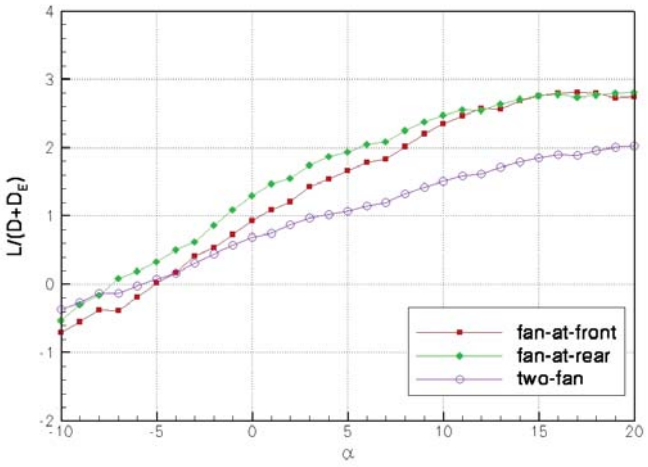

Figure 10. Equivalent lift over drag ratio. (μ = 0·227).

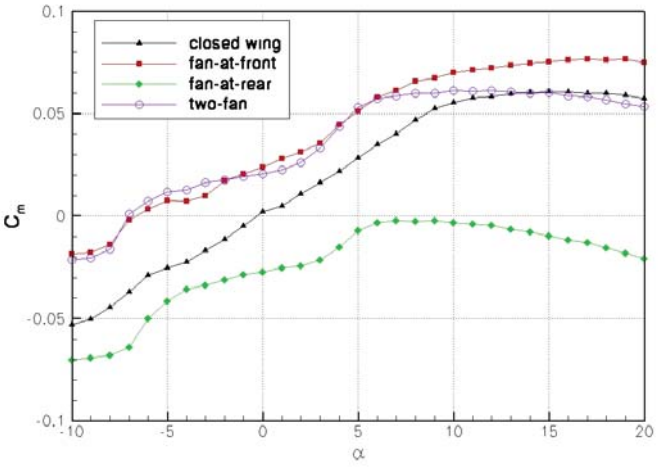

Figure 11. Pitching moment coefficient (μ = 0·227).

moments. No particular information was available on the fan thrust during the tests. Only static measurements, at zero airspeed, are performed. Hence, the fan thrust coefficient could then not be used for combining the effect of the freestream and rotational speed variation. Therefore the tip-speed ratio μ (Equation (1)), also used by Hickey[2], has been employed for the following analysis. Table 1 gives the correspondence between the average fan rotational speed and the freestream velocity.

Table 1
μ correspondence table

V_∞/N	21,000rpm	23,700rpm	26,500rpm
30ms^{-1}	0·227	0·201	0·180
40ms^{-1}	0·303	0·269	0·240
50ms^{-1}	0·379	0·336	0·300

Here, results are presented only for the fan-at-rear configuration. Fig. 12(b) shows the variation of C_D for several tip-speed ratios. Note that the Reynolds number varies to some extent for the different tip-speed ratios investigated. A decrease in μ (i.e. a rise of the rotor rpm) results in a rise of the drag coefficient. Between two values of μ, this reduction appears as a constant offset for the whole angle-of-attack range. Concerning now Fig. 12(a), a decrease in the tip-speed ratio causes an augmentation of the lift coefficient. Note that this phenomenon becomes less significant at high angle-of-attack. Further, a decrease in μ generates a nose down pitching moment coefficient for positive angles of attack (Fig. 12(c)).

To summarise our findings, the maximum lift, maximum drag and lower pitching moment are achieved for μ = 0·180 (V_∞ = 30ms^{-1} and N = 26,500rpm). The minimum lift, minimum drag and maximum pitching moment are obtained with μ = 0·379 (V_∞ = 50ms^{-1} and N = 21,000rpm). Thus the tip-speed ratio, μ, reflects the freestream capability to deflect the jet exiting the rear nozzle. This deflection has been observed in the wind tunnel using smoke visualisation technique. The value μ = 0·379 corresponds to the lower thrust and the highest freestream velocity investigated. In such operating conditions the jet is strongly swept back by the freestream resulting in a lower pressure drag but also resulting in less pressure increase upstream of the fan exit leading ultimately to a lower lift coefficient. The value μ = 0·180 corresponds to the maximum thrust available and the lower freestream velocity studied. The jet blockage effects, as well as the pressure drag, are more significant resulting in a higher lift coefficient, a larger nose down pitching moment and higher drag coefficient.

For the fan-at-front configuration, a change in μ has no significant effect on the lift coefficient.

Similar to the fan-at-rear configuration, a decrease in μ is linked to a rise in the drag coefficient. A nose up pitching moment is observed in this case. Thus, in a single fan in wing configuration, the model response to a change in μ depends on the fan streamwise location, affecting the performance in terms of lift and drag and also the longitudinal stability.

https://doi.org/10.1017/S0001924000002736 Published online by Cambridge University Press

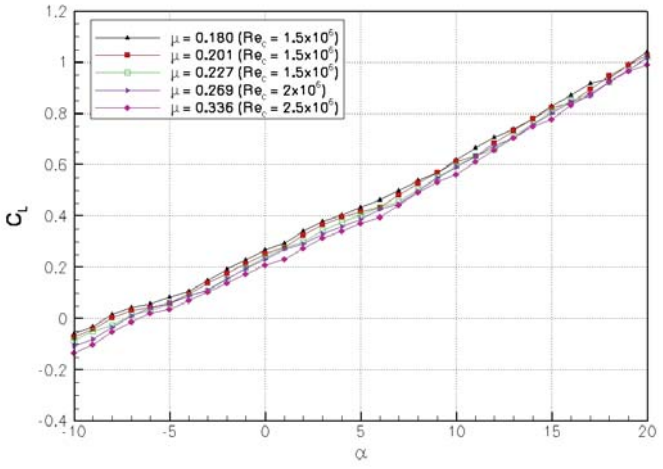

(a) lift coefficient

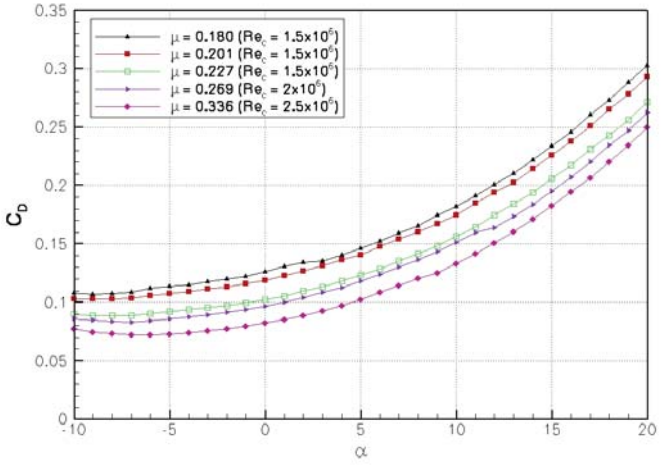

(b) drag coefficient

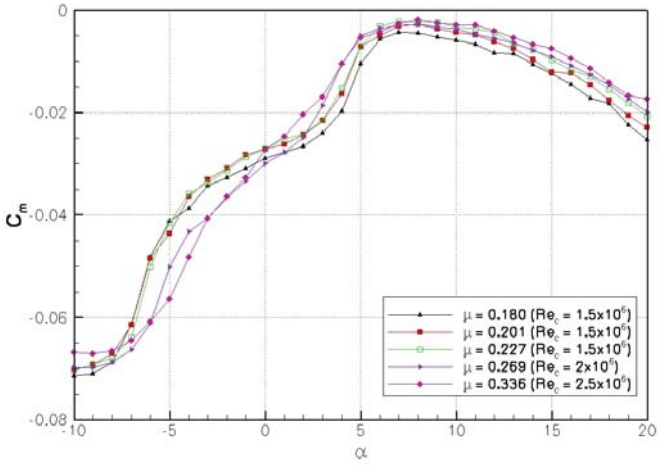

(c) pitching moment coefficient

Figure 12. Tip-speed ratio influence.

3.2 Pressure measurements

As previously mentioned, the pressure measurements are conducted within a stall free angle-of-attack range. Three different freestream velocities 30ms^{-1}, 40ms^{-1} and 50ms^{-1} and three fan rotational speeds 21,000rpm, 23,700rpm and 26,500rpm are investigated. This corresponds to nine different combinations associated to a unique tip-speed ratio, respectively (see Table 1).

3.2.1 Configuration comparison

In this section, a comparison of the configurations is discussed for $\mu = 0{\cdot}227$ and $\alpha = 0°$. At zero angle of incidence, the induced lift due to the angle-of-attack is zero and consequently the fan effect on the flow can be isolated. Only the chordwise pressure distribution located at ⅓s from the root chord is presented here for the four different configurations. For the reference configuration (Fig. 13(a)), a difference in the pressure coefficient is observed between the upper and lower side of the wing. This difference is due to a slight profile imperfection. According to section 3.1.1, the aerodynamic coefficients are in this case $C_L = 0{\cdot}006$, $C_D = 0{\cdot}014$ and $C_m = 0{\cdot}002$. Comparing this reference measurement to the fan-at-rear position (Fig. 13(c)), we can see that the fan strongly affects the flow. On the wing upper side the suction is improved by the fan. It is especially true in the fan vicinity. On the wing lower side, the pressure increases upstream of the nozzle due to the blockage effect of the nozzle jet. The pressure coefficient drops dramatically at 60% of the chord, corresponding approximately to the fan location. An area with low pressure coefficient is created downstream of the nozzle. The circulation is improved by the fan located at the wing rear part and the lift coefficient is notably increased. The corresponding aerodynamic coefficients are $C_L = 0{\cdot}24$, $C_D = 0{\cdot}102$ and $C_m = -0{\cdot}03$. Though, the region with low pressure coefficient induces a loss in lift and an increase in the pressure drag downstream of the nozzle and on the wing lower side.

On Fig. 13(b), it is shown the chordwise pressure distribution for the fan-at-front configuration. The fan position in a single fan in wing configuration has clearly an effect on the aerodynamic coefficients as previously stated ($C_L = 0{\cdot}16$, $C_D = 0{\cdot}088$ and $C_m = 0{\cdot}02$). Compared to the reference case, the suction is enhanced only in a small region upstream of the inlet lip on the wing upper side. On the wing lower side, the drop in C_p occurs logically upstream at approximately 20% of the chord.

After analysing the single fan-in-wing chordwise pressure distribution, the focus is now on the two-fan configuration. According to Fig. 13(d), the pressure coefficient remains approximately constant from 10 % to 60% of the chord on the wing upper side. Thus, the fan suction seems to be more homogeneous in this configuration and acts on a wider area. On the wing lower side, the drop in pressure coefficient occurs at 20% of the chord as observed for the fan-at-front configuration. The corresponding force and moment measurements are $C_L = 0{\cdot}20$, $C_D = 0{\cdot}133$ and $C_m = 0{\cdot}02$. Theses graphs give now a clear interpretation of the force measurements. In terms of circulation enhancement, the fan-at-rear configuration remains the most efficient configuration. In this configuration, the jet exiting the rear nozzle creates a jet flap effect consequently reducing the mass flow rate on the wing lower side. As a result the pressure is increased upstream of the nozzle. It is shown again that, located at the trailing edge, the fan increases effectively the lift coefficient. However, the jet at the rear position is less deflected by the freestream than a jet exiting at the front and therefore generates more pressure drag.

3.2.2 Tip-speed ratio effect

Here, the focus is on the fan-at-rear configuration. The effect of tip-speed ratio is studied referring directly to paragraph 3.1.2.

https://doi.org/10.1017/S0001924000002736 Published online by Cambridge University Press

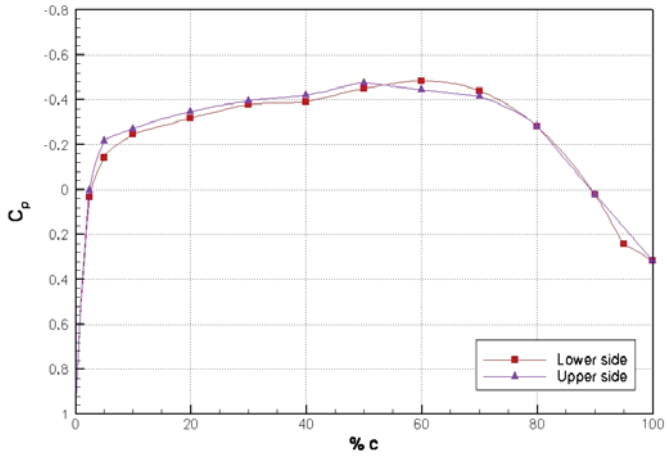

(a) closed wing

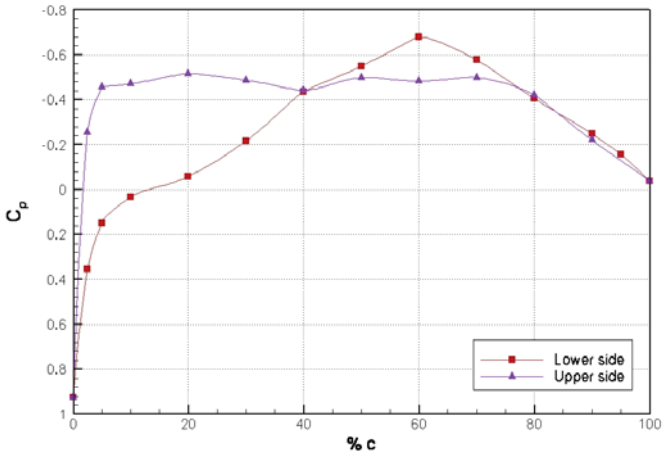

(b) fan at front

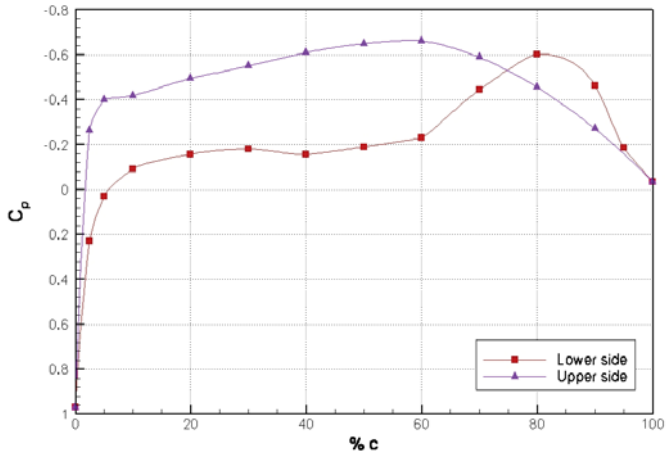

(c) fan at rear

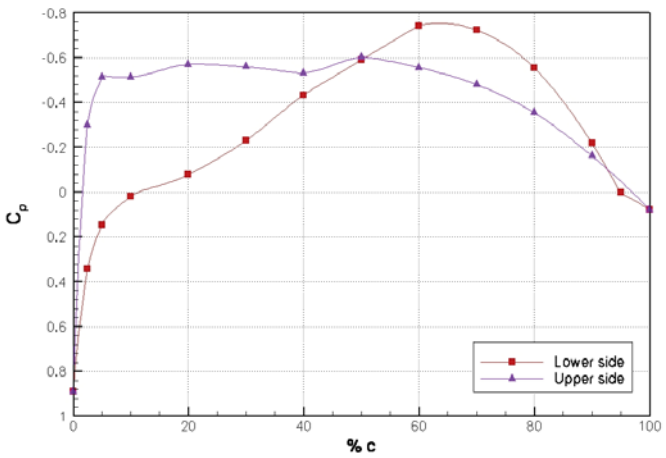

(d) two fans

Figure 13. Chordwise pressure distribution at ⅓s (for μ = 0·227 and α = 0°).

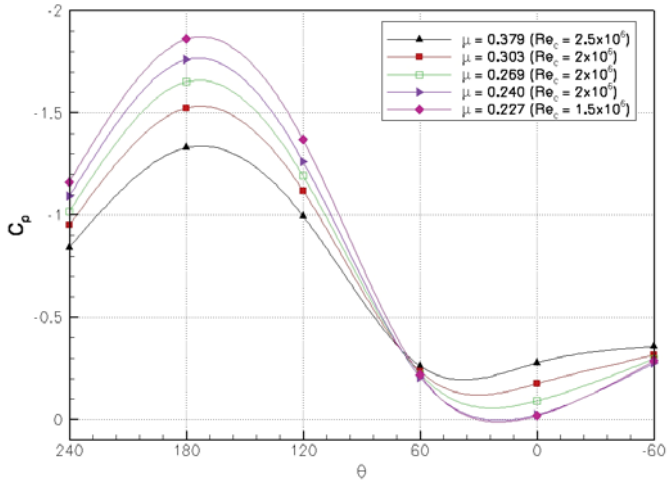

(a) on the wing upper side

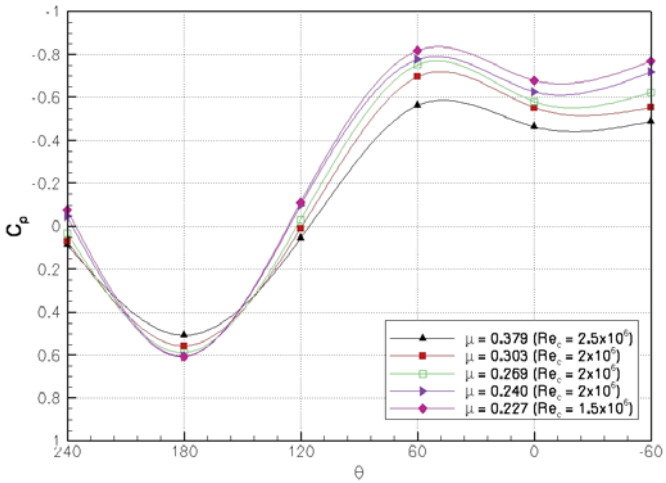

(b) on the wing lower side

Figure 14. Circumferential pressure distribution at 1·6*R* around the rear fan (for μ = 0·227 and α = 0°).

https://doi.org/10.1017/S0001924000002736 Published online by Cambridge University Press

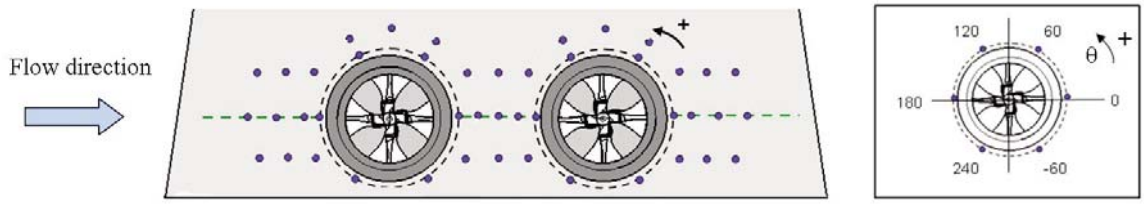

(a) Pressure taps layout

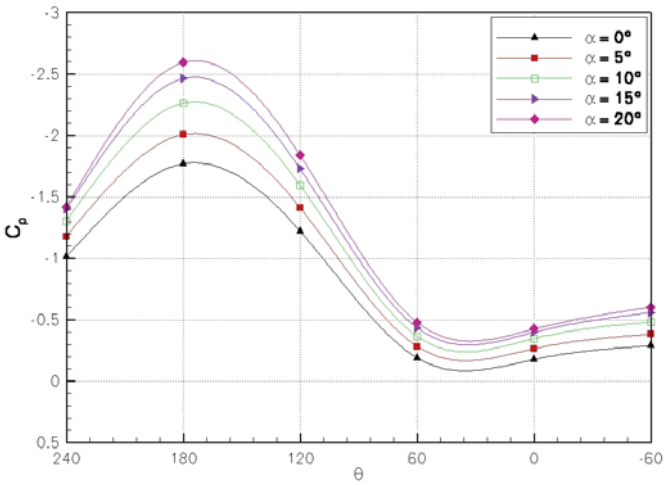

(b) around the front fan, on the wing upper side

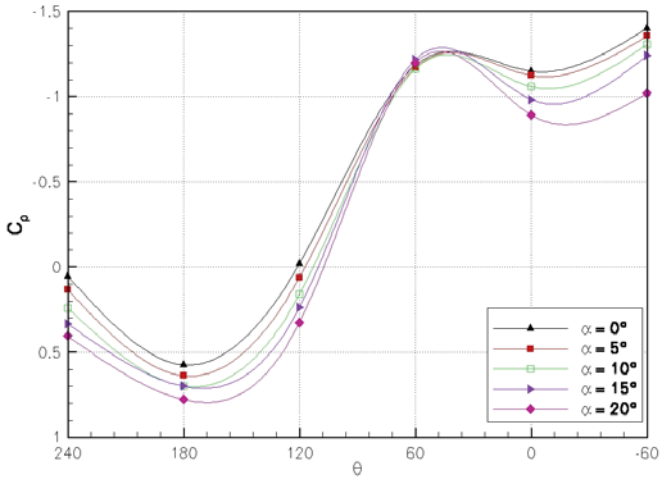

(c) around the front fan, on the wing lower side

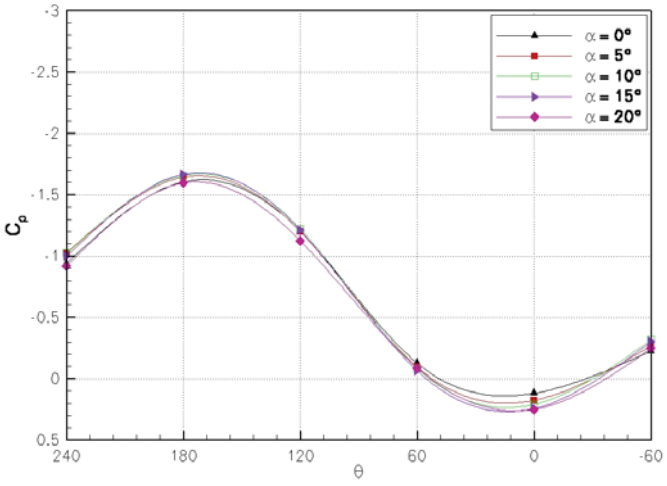

(d) around the rear fan, on the wing upper side

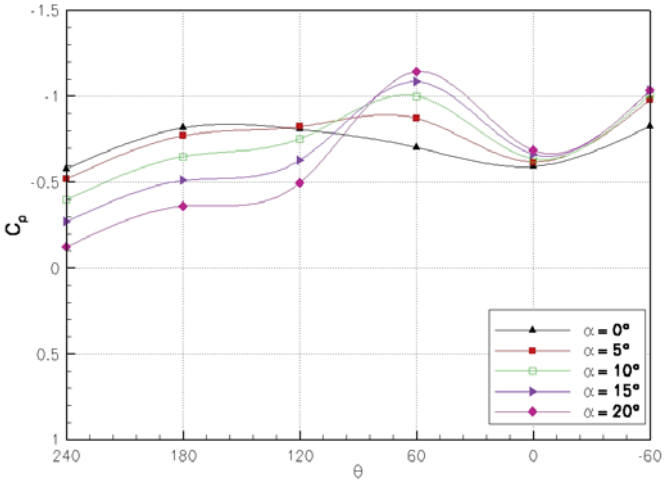

(e) around the rear fan, on the wing lower side

Figure 15. Circumferential pressure distribution at 1·6 R (for μ = 0·227).

According to Fig. 14(a), a decrease in the tip-speed ratio induces a lower pressure coefficient upstream of the fan (roughly θ in the interval [90,240]) on the wing upper side. This occurs significantly in the vicinity of the fan on the inlet lip.

The circumferential pressure distribution on the wing upper side indicates that the inflow pressure distribution is highly inhomogeneous. This corresponds to a high speed region located around θ = 180° and region of low speed in the vicinity of θ = 0°. Thus, this non-uniform pressure distribution tends to create non uniform load on the rotor blades and therefore a less efficient use of the fan, hence producing less thrust. The addition of inlet guide vanes could improve the air ingestion by the fan and enable a more uniform velocity distribution at the inlet. Inlet guide vanes enhance the lift and each guide vane angle has to be adjusted independently to avoid separation on the vane blades[2]. The inlet lip to diameter ratio and the inflow depth are also critical parameters affecting the flow field at the fan inlet[10]. According also to Fig. 14(a), one can note that $C_p(\theta = -60°) < C_p(\theta = 60°)$ and $C_p(\theta = 120°) < C_p(\theta = 240°)$. The asymmetric pressure distribution is linked to the counter clockwise rotation sense of the rotor with respect to the plane located at 0·12s. On the wing lower side, a drop in μ provokes a slight pressure coefficient increase for θ = –180° (Fig. 14b). Downstream of the nozzle, C_p decreases significantly (θ in the interval [–60, 60]). This graph suggests that lower values of tip-speed ratio generate more pressure drag. These results are consistent with the force measurements.

https://doi.org/10.1017/S0001924000002736 Published online by Cambridge University Press

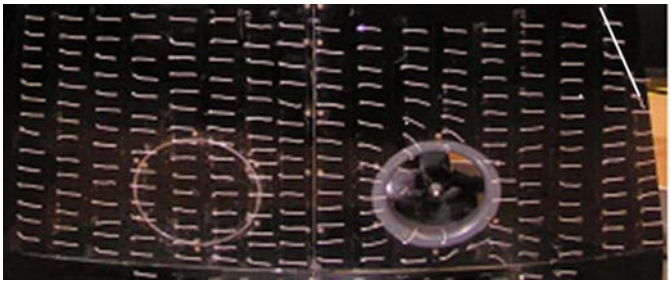

(a) fan-at-rear (α = 0°)

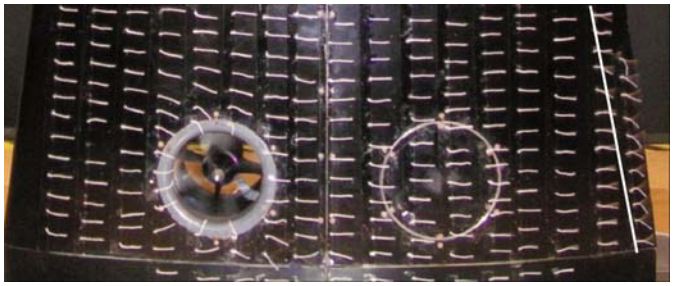

(b) fan-at-front (α = 0°)

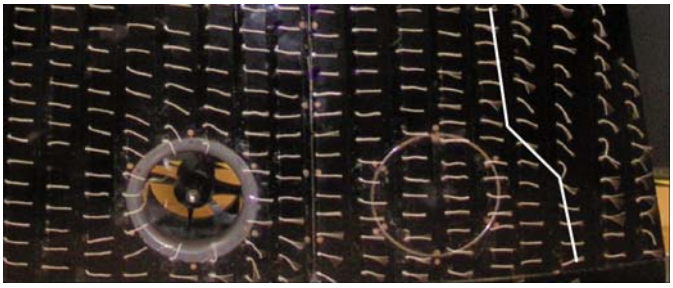

(c) fan-at-front (α = 20°)

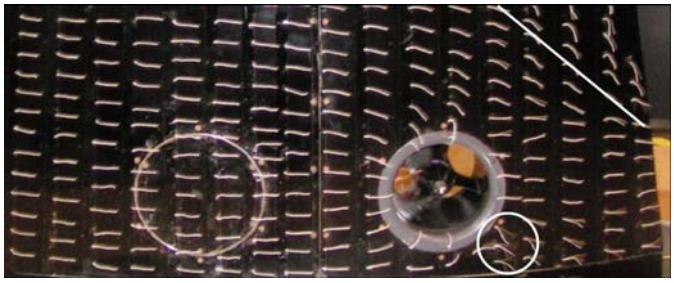

(d) fan-at-rear (α = 20°)

Figure 16. Wool-tufts visualisation on the wing upper side

3.2.3 Jet Interference in the two- fan configuration

As previously discussed, the fan position has an important influence with respect to a tip-speed ratio change in one single fan-in-wing configuration. The circumferential pressure distribution investigation for the two fans configuration can also give some insight on the interference of the jets with respect to an angle-of-attack variation. The results presented here are for a tip-speed ratio μ = 0·227 (V_∞ = 30ms^{-1}and N = 21,000rpm). For clarity, the pressure taps layout is recalled in Fig. 15(a). On the wing upper side, the circumferential pressure distribution (at 1·6R) around the front fan (Fig. 15(b)) indicates an increase in suction while raising the angle-of-attack. For the rear fan, the increase in α has almost no influence on the pressure coefficient (Fig. 15(d)). This result is also valid for the single fan-at-rear configuration. No significant change in C_p is observed on the wing upper side in the vicinity of the rear fan with an increase in α.

On the wing lower side and for the front fan (Fig. 15(c)), the increase in α implies a rise in C_p. In the region upstream of the rear nozzle exit (θ in the interval [90,240]), the pressure coefficient also increases. Downstream of the nozzle, the circumferential pressure distribution shows two peaks located at θ = 60° and θ = –60°, Fig. 15(c) and (e). These peaks, which correspond to a lower value of the pressure coefficient, reflect the presence of vortices on each side of the jet. This effect is present for all circumferential pressure distributions around the fan exit. The suction peaks appear more clearly at high angle-of-attack, Fig. 15(e). Note that the front jet interferes with the rear jet, as shown by the inflection point located at about θ = 90°. This inflection point has not been observed for the other fan-in-wing configurations.

All these results are corroborated by the second circumferential pressure distribution (at 1·9R). The interference between the front and rear jet gives some more understanding of the drag coefficient measurement. At high angle-of-attack, the front jet is significantly swept back and interacts with the rear jet. Above α = 14° the drag coefficient becomes less important for the two-fan than for the fan-at-rear configuration.

3.3 Wool-tufts flow visualisation

Qualitative flow visualisation results are presented for the three different fan-in-wing configurations at selected operating conditions.

3.3.1 Wing upper side

In this section the wool-tufts flow visualisations are presented for μ = 0·180 (V_∞ = 30ms^{-1} and N = 26,500rpm). At 0° angle-of-attack, trailing edge separation has been observed on the closed wing at approximately 95% c. When a single fan is placed at the rear (Fig. 16(a)), no separation is observed at the trailing edge downstream of the fan at α = 0°. The separation however occurs at the trailing edge when approaching the wing tip.

Thus, the fan at rear prevents the trailing edge separation on the wing upper side in a region downstream of the fan. When a single fan is placed at the front (Fig. 16(b)), the separation at the trailing edge is not avoided. For the two-fan configuration, no separation is observed at the trailing edge due to the presence of the rear fan.

Note that a small separation area (located at θ = –60°), circled on Fig. 16(d), is observed close to the fan. This effect occurs for all operating points and configurations. It is related to the transitional zone of low momentum where the streamlines are ingested. This area of flow separation is however not observed on the other side of the fan (around θ = 60°). The incoming flow combined with the counterclockwise rotation of the fan creates a retreating and advancing condition on the rotor blades. It explains the asymmetric behavior of the separation near the inlet lip. The pressure tap at θ = –60° is located in this separated area and shows lower pressure as at θ = 60°. Parameters such as inflow depth over the rotor blade, inlet lip radius to diameter ratio, may also have an influence on this phenomenon.

At 20° angle-of-attack, the separation area at the trailing edge on the upper side is extended, Fig. 16(c). The trailing edge separation is slightly moved upstream for the fan-at-front configuration in a region located behind the fan. Contrary, the fan-at-rear configuration keeps the flow attached at the trailing edge but only in a small area downstream of the fan. As shown in Fig. 16(d), the separation appears in the spanwise direction outboard of the fan.

As previously stated, all configurations experience stall at α = 26°. The fan pumping behavior of all fan-in-wing configurations confirm

https://doi.org/10.1017/S0001924000002736 Published online by Cambridge University Press

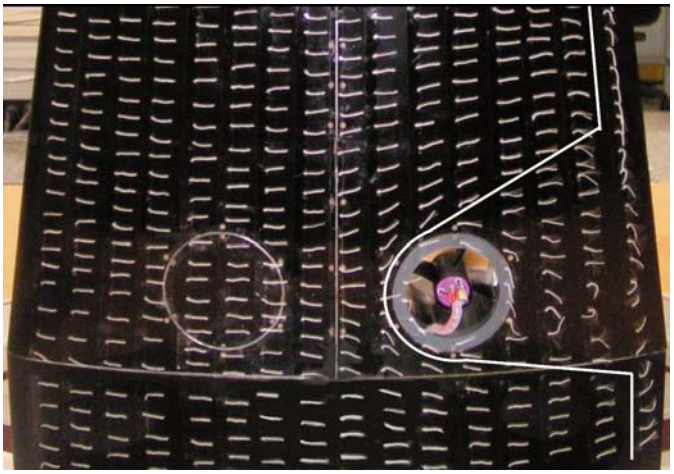

(a) fan-at-rear

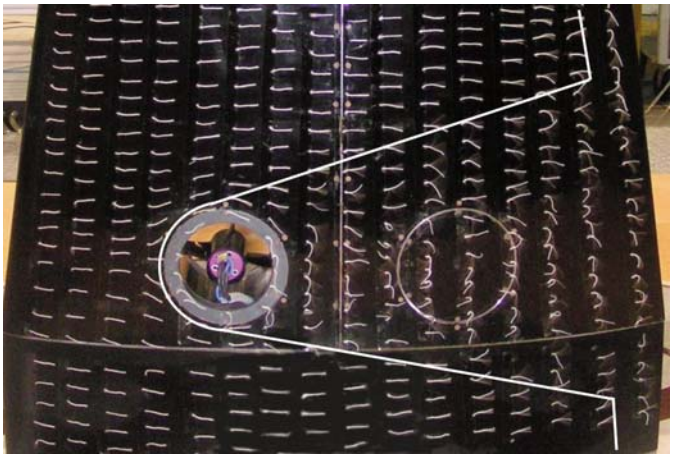

(b) fan-at-front

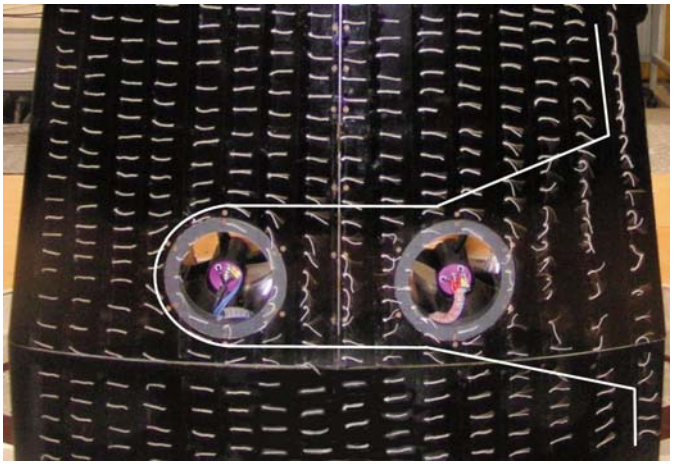

(c) two-fan

Figure 17. Wool-tufts visualisation on the wing lower side (at α = 0°).

this statement. Although the fan located at the rear part of the wing clearly prevents the separation at the trailing edge, the stall cannot be avoided and occurs at the same angle-of-attack than for the closed wing. Thus, the fan can act as a device for flow control, on the wing upper side, if located near the trailing edge and only in a region downstream of the fan.

3.3.2 *Wing lower side*

As indicated by the pressure measurements, a suction area on the wing lower side is created downstream of the fan nozzle due to the jet mixing with the cross flow. The size of the wing part affected depends on the fan location. For the fan-at-front (Fig. 17(b)) and fan-at-rear (Fig. 17(a)) configurations, this area affected by the mixing occurs slightly upstream of the fan and tends to spread conically downstream of the nozzle. The flow is highly unsteady on the wing lower side. Therefore, the wool tufts visualisation does not allow us to clearly identify the region of attached and separated flow. The two-fan configuration indicates a different pattern with a straight affected area between the two fans, Fig. 17(c). Again, the mixing of the jet with the cross flow observed downstream of the nozzle penalises significantly the model performance. This is mainly characterised by a significant lift loss due to high suction on the wing lower surface downstream of the fan exit. The adverse pressure gradient generated by the jet exiting the nozzle causes the wall boundary-layer to separate. Therefore, a horseshoe vortex is created upstream of the fan exit (Fig. 17(a-c)).

3.4 Flow field measurements

The PIV measurements are performed near the wing trailing edge downstream of the nozzle for the fan-at-rear configuration to capture the disturbance pointed out by the pressure measurements and the wool-tufts flow visualisation. The tip-speed ratio investigated here is μ = 0·240 (V_∞ = 40ms^{-1} and N = 26,500rpm). The PIV image corresponding to Fig. 18, shows the streamwise velocity distribution in a cross-flow plane located at 1·22c. The jet exiting the fan nozzle rolls up into a pair of counter-rotating vortices. At 1·22c, the pair of vortices shows a well formed 'kidney shape'. Backward velocity can be expected close to the nozzle exit in the vortex core, as displayed in the wool tufts visualisation (Fig. 17(a)). The 'V-shape' over the pair of vortices (contour of $u \approx$ 30ms^{-1}) corresponds to the trailing edge wake. For the wing without fan, the wake would be nearly straight approximately located at z = 0mm. The pair of vortices has the tendency to convect in negative z direction while going downstream. Consistent with the chordwise pressure measurements, the cross flow mixing at the fan exit induces a downwash on the wing part located downstream of the nozzle, consequently resulting in a loss of lift. According to the previous discussion, the shape of these vortices and the magnitude of the induced velocities depend mainly on the angle-of-attack, the configuration, and tip-speed ratio.

4.0 CONCLUSION

A generic fan-in-wing configuration has been investigated experimentally. Force, pressure and PIV measurements as well as flow visualisation have been performed to study the aerodynamic characteristics. The main results are as follows:

1) The presence of a fan rotating in the wing plane enhances the suction on the wing upper side and particularly in the vicinity of the inlet lip. The jet leaving the nozzle is swept back by the freestream and rolls up into a pair of counter-rotating vortices. Due to the blockage effect upstream of the nozzle, the pressure is increased on the wing lower side, similarly to a jet flap. A horseshoe vortex is created upstream of the fan exit due to this adverse pressure gradient. Consequently, the lift coefficient is increased compared to the reference configuration without fans.

https://doi.org/10.1017/S0001924000002736 Published online by Cambridge University Press

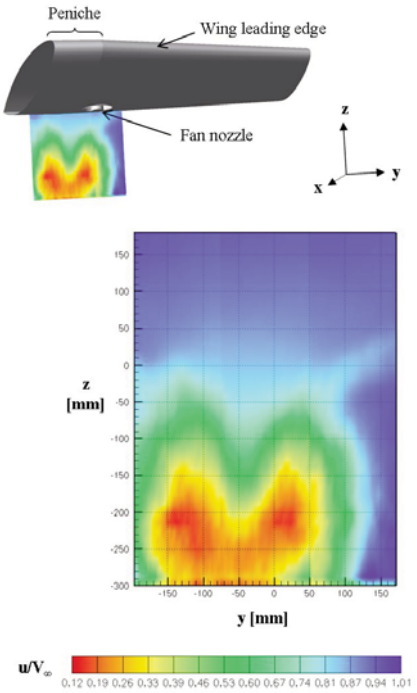

Figure 18. Streamwise velocity distribution. The picture center (y = 0mm and z = 0mm) is located at x = 1·22c, y = 0·18s, and z = –0·14t from the root chord leading edge. α = 0°, V_∞ = 40ms^{-1}, N = 26,200 rpm (μ = 0·243).

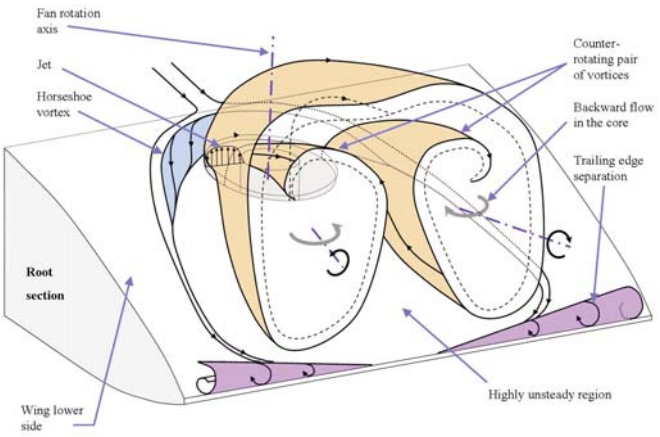

Figure 19. Flow phenomenology on the wing lower side.

Depending on the fan position a more or less wide disturbance region downstream of the fan exit, characterised by low pressure coefficients, is created behind the jet. As a result a drop in lift and a rise in pressure drag are observed. The findings concerning the flow topology on the wing lower side are summarised in Fig. 19.

2) The ratio of the freestream velocity and fan rotational speed is used as a non-dimensionalised coefficient and reflects the freestream capability to deflect the jet. If the jet is strongly swept back, the lift and drag coefficients are reduced. The fan position is also important. The jet created by the fan-at-front configuration is swept backward more than by the fan-at-rear position. This effect is particularly true at high angle-of-attack and, therefore, this has an influence on the pressure drag. The single fan installed in the rear configuration remains more efficient than the others in terms of circulation improvement. The lift coefficient increases with moving the position of the fan to the trailing edge.

3) The flow ingested by the fan is highly inhomogeneous with a low pressure coefficient upstream of the inlet lip and a stagnation region downstream. The inflow is highly distorted resulting in a less efficient use of the fan with non uniform loads.

The influence of the fan position has been studied as well as the jet interference in a configuration where two fans are placed one next to the other in the streamwise direction. This paper has highlighted also the issues encountered in this configuration: large suction area downstream of the nozzle on the wing lower side, highly distorted inflow. Overall, this study clearly demonstrates the enhancement of the flow circulation by the fan and the induced lift that could be beneficial for a STOL regional aircraft. Many improvements can be made to the present configuration to optimise the model performance in terms of inlet and outlet guide vanes, and optimising inflow depth and inlet lip radius to diameter. A broad range of experimental results have been obtained to be used as reference data for code validation.

5.0 FUTURE WORK

The fan-at-rear configuration presented in this paper has been studied numerically, based on a block structured mesh including the fan. URANS using a sliding mesh to simulate the fan rotation will be conducted. The data obtained within this experiment allow us to evaluate the CFD simulations accuracy for this unconventional flow problem. As a further step, a parameter study will be conducted numerically. This parameter study will include the analysis of different disk loading and tip-speed ratios to provide additional design sensitivities. Guiding elements and deployable seal will be also studied numerically.

ACKNOWLEDGMENTS

This research was funded by the Bauhaus Luftfahrt e.V which is gratefully acknowledged. The authors would like to express their gratitude to Mr Florian Vogel for his help in performing the PIV measurements.

REFERENCES

1. GOLOGAN, C. Conceptual design of a STOL regional-jet with hybrid propulsion system, Proceeding of the International Congress of the Aeronautical Sciences, Anchorage, USA, September 2008.
2. HICKEY, D.H. and ELLIS, D.R. Wind tunnel tests of a semispan wing with a fan rotating in the plane of the wing, NASA TN-D88, 1959.
3. HICKEY, D.H. and HALL, L.P. Aerodynamic characteristics of a large-scale model with two high disk-loading fans mounted in the wing, NASA TN-D1650, USA, 1963.
4. HALL, L.P., HICKEY, D.H. and KIRK J.V. Aerodynamic characteristics of a full-scale fan-in-wing model including results in ground effect with nose-fan pitch control, USA, NASA-TN-D-2368, 1964.
5. KIRBY, R.H. and CHAMBERS, J.R. Flight investigation of dynamic stability and control characteristics of a 0.18-scale model of a fan-in-wing VTOL airplane, NASA-TN-D-3412, USA, 1966.

https://doi.org/10.1017/S0001924000002736 Published online by Cambridge University Press

6. OBERTO, R.J., RENSELAER D.J. and ALFANO, D.L. Analysis of performance characteristics in ground effect of a large scale V STOL multi-fan-in-wing transport model, NASA-CR-1180, USA, 1968.
7. HEYSON, H.H. The effect of wind tunnel wall interference on the performance of a fan-in-wing VTOL model, NASA-TN-D-7518, USA, 1974.
8. WILSON, J.C., GENTRY, G.L. and GORTON S.A. wind tunnel test results of a 1/8-scale model, NASA TM-4710, USA, 1996.
9. SCHADE, R.O. Ground interferences effects, NASA-TN-D-727, 1961.
10. SCHAUB, U.W. Experimental investigation of flow distortion in fan-in-wing inlets, *J Aircr*, 1968, **5**, (5), pp 473-478.
11. HODDER, B.K., KIRK, J.V. and HALL, L.P. Aerodynamic characteristics of large-scale model with a lift fan mounted in a 5-percent-thick triangular wing, including the effects of BLC on the lift-fan-inlet, NASA TN D-7031, 1970.
12. LIEBLEIN, S., YUSKA, J.A. and DIEDRICH, J.H.. Performance characteristics of a model VTOL lift fan in crossflow, *J Aircr*, **10**, (3), 1973, pp 131-136.
13. HICKEY, D.H. and COOK, W.L. Aerodynamics of V/STOL aircraft powered by lift fans, AGARD CP 22, (15), September 1967.
14. HICKEY, D.H. and KIRK, J.V. Studies of forces induced on V/STOL aircraft by propulsion flows, proceedings of the NASC workshop propulsion aerodynamics, 28-31 July, 1975.
15. HICKEY, D.H. and KIRK, J.V. Survey of Lift-fan aerodynamic Technology, NASA CR 177615, USA, 1993.
16. DIEDRICH, J.H. Summary of model VTOL lift fan tests conducted at NASA Lewis Reseach Center, NASA TM X-71778, USA, 1975.
17. PRZEDPELSKI, Z.J. Lift fan technology studies, NASA CR-761, USA, 1967.
18. LIEBLEIN, S. A review of lift fan propulsion systems for civil VTOL transports, NASA TM X-52829, USA, 1970.

https://doi.org/10.1017/S0001924000002736 Published online by Cambridge University Press